Crystalline lens radii of curvature from Purkinje and Scheimpflug imaging

Patricia Rosales Instituto de Optica, "Daza de Valdés," Consejo Superior de Investigaciones Científicas, Madrid, Spain

Michiel Dubbelman Department of Physics and Medical Technology, VU University Medical Center, Amsterdam, The Netherlands

Susana Marcos Instituto de Optica, "Daza de Valdés," Consejo Superior de Investigaciones Científicas, Madrid, Spain

Rob van der Heijde Department of Physics and Medical Technology, VU University Medical Center, Amsterdam, The Netherlands

We present a comparison between measurements of the radius of the anterior and posterior lens surface, which was performed using corrected Scheimpflug imaging and Purkinje imaging in the same group of participants (46 for the anterior lens, and 34 for the posterior lens). Comparisons were also made as a function of accommodation (0 to 7 D) in a subset of 11 eyes. Data were captured and processed using laboratory prototypes and custom processing algorithms [for optical and geometrical distortion correction in the Scheimpflug system and using either equivalent mirror (EM) or merit function (MF) methods for Purkinje].

We found statistically significant differences in 4 of 46 eyes for the anterior lens radius, and 10 of 34 eyes for the posterior radius (using the MF and individual biometric data to process the Purkinje images). For the anterior lens, the agreement increases using individual biometry as opposed to biometric data from a model eye. For the posterior lens, the agreement increases using the MF as opposed to the EM method. For the changes during accommodation, no significant difference between the two techniques was found.

In conclusion, the results of the cross-validation using the Scheimpflug and Purkinje imaging technique show that both techniques provide comparable lens radii and similar changes with accommodation. Purkinje tends to overestimate posterior lens radius, whereas pupil size limits the acquisition of posterior lens data with the Scheimpflug camera. Computer simulations using the Scheimpflug data as input show that the consistent slight overestimation of the posterior lens radius using Purkinje imaging can be partly attributed to the asphericity of the lens surface.

Keywords: crystalline lens, Scheimpflug, Purkinje, radii of curvature, phakometry, accommodation

Introduction

Accurate measurements of the radii of curvature of the crystalline lens surfaces, in combination with other measurements, such as lens thickness, lens index of refraction, or anterior chamber depth, are essential for a better understanding of the accommodation mechanism and the origin of presbyopia. Furthermore, knowledge on the shape of the crystalline lens is necessary to understand the sources of optical aberrations in the eye (Marcos, Burns, Moreno-Barriuso, & Navarro, 1999) and to evaluate the relative contribution of lens geometry and refractive index distribution to the optical changes occurring during aging (Guirao & Artal, 2000; Guirao, Redondo, & Artal, 2000; Marcos, Barbero, McLellan, & Burns, 2004) or accommodation (Glasser, Wendt, & Ostrin, 2006; He, Gwiazda, Thorn, Held, & Vera-Diaz, 2005; Roorda & Glasser, 2004). Finally, a better knowledge of the crystalline lens geometry is important in the field of intraocular lens design (Holladay, Piers, Koranyi, van der Mooren, & Norrby, 2002; Marcos, Barbero, & Jiménez-Alfaro, 2005).

Purkinje imaging has been one of the most popular methods to perform phakometry. Purkinje images, first described by Purkinje in 1832, are reflections from the ocular surfaces. The radii of curvature of the different ocular components (acting as mirrors) are estimated from the relative height of images of the light source. The brightest reflection (first Purkinje image, PI) comes from the anterior corneal surface and can be used to estimate the corneal radius of curvature, as it is done in keratometry. The third (PIII) and fourth Purkinje images (PIV), from the anterior and posterior surface of the crystalline lens, are used for phakometry. Two algorithms have been proposed to estimate the radii of curvature from the relative heights of PIII and PIV: the equivalent mirror (EM) theorem method, based on the replacement of the different ocular surfaces by a single mirror (Smith & Garner, 1996), and the merit

doi: 10.1167/6.10.5 Received March 14, 2006; published September 19, 2006 ISSN 1534-7362

function (MF), based on a recursive method (Barry, Dunne, & Kirschkamp, 2001; Garner, 1997). Recent computer simulations of an experimental Purkinje imaging system developed in our laboratory show that the MF produced more accurate results for the posterior surface than EM (Rosales & Marcos, 2006). Early Purkinje imaging systems were based on photography (Van Veen & Goss, 1988; Wulfeck, 1955) and some versions were used to study correlations between refractive error and geometrical properties of the lens (Sorsby, Benjamin, & Sheridan, 1961). Mutti, Zadnik, and Adams (1992) used it to study myopia and to study normal ocular development in children population (Zadnik et al., 2004). Additional technical implementations include the use of a telecentric stop lens to capture PI, PIV, and PIII (in a slightly different plane) with no magnification changes (Phillips, Perez-Emmanuelli, Rosskothen, & Koester, 1988). This method was used to measure the refractive index with age (Garner, Ooi, & Smith, 1998; Hemenger, Garner, & Ooi, 1995), with accommodation (Garner & Smith, 1997), and the change in lens radius with accommodation (Garner & Yap, 1997).

Another technique to measure the shape of the lens is Scheimpflug imaging, which provides a sharp image of the entire anterior eye segment. A Scheimpflug camera can be regarded as a modified slit lamp in which the image plane, lens plane, or both planes are tilted to obtain a sharp image of the cornea and lens simultaneously (Scheimpflug, 1906). The technique has been widely used to measure the shape of the lens with age and accommodation (Brown, 1974; Dubbelman & Van der Heijde, 2001; Dubbelman, Van der Heijde, & Weeber, 2005; Koretz, Cook, & Kaufman, 1997, 2001, 2002; Koretz & Handelman, 1986). To extract reliable quantitative results on lens shape from Scheimpflug images, special care must be taken to correct the images for two types of distortion. The first distortion is due to the geometry of the Scheimpflug imaging system because the object and image planes are not parallel to each other. This introduces a variation of the magnification along the image plane, which can be corrected analytically (Ray, 1995). The second type of distortion is due to the refraction at the various intraocular surfaces. Thus, measurement of the anterior lens surface has been influenced by the refraction of the cornea, and the measurement of the posterior lens surface has additionally been influenced by the optics of the lens itself. This type of distortion can only be corrected by applying ray tracing to every pixel of each individual Scheimpflug image to find its real coordinates (Fink, 2005; Huebscher, Fink, Steinbruck, & Seiler, 1999; Kampfer, Wegener, Dragomirescu, & Hockwin, 1989).

Despite Scheimpflug and Purkinje imaging being the most popular alternatives to perform in vivo phakometry, to our knowledge a direct comparison between radii of curvature obtained with these two techniques on the same eyes has never been done. Koretz, Strenk, Strenk, and Semmlow (2005) performed a comparative study between Scheimpflug and high-resolution magnetic resonance imaging (MRI) of the anterior segment of the eye. In this study each technique was performed on a different group of participants and only a comparison could be made on the trends of the cross-sectional changes with age. Furthermore, there has been discussion on the statistical methods used and the conclusions drawn from the results (Dubbelman et al., 2005).

In this study, we compare phakometry from Purkinje imaging (developed at the Instituto de Optica, Madrid, Spain) and from Scheimpflug imaging system (implemented at VU Medical Center, Amsterdam) on the same set of participants for relaxed accommodation, and as a function of accommodation in a subsample of eyes.

Methods

Purkinje imaging

A Purkinje imaging system, developed at the Instituto de Optica, Madrid, Spain, was used to perform phakometry. The optical set-up, data analysis, as well as experimental and computational validations have been described in detail in a previous publication (Rosales & Marcos, 2006). The system is very compact and was easily transported to the VU University Medical Center, Amsterdam, The Netherlands, where the experiments were conducted. The patient's eye was illuminated by two sets double infrared (IR) LEDs (for right and left eye respectively), separated 12 mm, mounted at a distance of 90 mm from the eye, at an angle of 15°. Pupillary images were captured on an IR-enhanced CCD camera provided with a 55-mm focal length telecentric lens mounted at a distance of 150 mm from the eye and focused at the pupil plane. An additional channel incorporates a fixation stimulus, presented on a minisplay. The system is also provided with two channels to perform lens tilt and decentration measurements, and with a Badal system to compensate for the eye's refractive error and induce accommodation, which were not used in the study reported here. Custom-developed software written in Visual Basic allowed automatic control of the system. For comparative measurements with the Scheimpflug system, a slight change was incorporated with respect to previous experiments: a mirror was inserted in the fixation channel to offer the left eye an accommodation stimulus while the right eye is being imaged.

Heights of the double Purkinje images were computed and processed to obtain radii of curvature in the vertical meridian. The anterior and posterior lens radius were obtained using both the EM (Smith & Garner, 1996) and the MF methods (Garner, 1997), with custom-developed routines written in Matlab. In brief, the EM establishes that different dioptric surfaces followed by a catoptric surface

can be replaced by a single mirror with an equivalent radius of curvature. The theorem is applied twice: (1) for the anterior lens, anterior and posterior corneal surfaces and anterior lens surfaces are replaced by a single mirror with an equivalent radius of curvature; (2) for the posterior lens, anterior and posterior corneal surfaces and anterior and posterior lens surfaces are replaced by a single mirror with an equivalent radius of curvature. The MF method uses as input the experimental heights of the double PIII relative to double PI and experimental heights of the double PIV relative to double PI. Theoretical relative Purkinje images heights are obtained recursively simulating a ray tracing through the different ocular surfaces assuming initial values for anterior and posterior lens radii of curvatures in an eye model. In this study, we use individual corneal radii of curvature from keratometry and biometric axial data (anterior chamber depth and lens thickness), either from Scheimpflug imaging or fixed data from a general model eye (Le Grand & El Hage, 1980). In a previous study (Rosales & Marcos, 2006) with our custom-developed Purkinje system, we used biometric data from optical biometry to process the data. Here we used optical biometry from Scheimpflug imaging or constant data from a model eye and both results are reported.

The Purkinje imaging system has been validated through computer simulations as well as in vivo with nine eyes with implanted IOLs with known powers, comparing those with estimates from measured the radii of curvature (Rosales & Marcos, 2006). Computer simulations of the Purkinje imaging system on eye models consistent with the assumptions of the method demonstrated an expected accuracy <0.3 mm for the anterior radius of curvature with both the EM and MF methods and 1 mm (EM) and 0.3 mm (MF) for the posterior radius respectively. On realistic eye models (with real corneal topography, gradient refractive index, aspheric lens surfaces), we estimated accuracy of 0.85 mm (EM) and 0.66 mm (MF) for the anterior lens radius and of 1.35 mm (EM) and 0.75 mm (MF) for the posterior lens radius.

Scheimpflug imaging

The set-up of the Scheimpflug camera as well as the necessary corrections of the Scheimpflug images, implemented at the VU Medical Center in Amsterdam, have been described previously in detail (Dubbelman, Sicam, & Van der Heijde, 2006; Dubbelman, van der Heijde, & Weeber, 2001; Dubbelman et al., 2005). Images were obtained with the Topcon SL-45 Scheimpflug camera, the film of which was replaced by a CCD camera (St-9XE, SBIG astronomical instruments) with a dynamic range of 16 bits of grey values (512 × 512 pixels, pixel size 20 × 20 μm, magnification: 1×). Correction and analysis of the Scheimpflug images are done using custom-developed software written in C++. A conic of revolution was fitted to the anterior and posterior lens surface to find the asphericity of the surfaces. Furthermore, a circle was fitted to the central 3-mm zone of both lens surfaces and it is this radius that will be compared with the results of the Purkinje imaging (Dubbelman & Van der Heijde, 2001). As a result, at least 3 mm of the lens surface should visible on the Scheimpflug image to obtain its radius. For the posterior lens surface, this was not always the case, especially when only phenylephrine was used to dilate the pupil. Dubbelman and Van der Heijde (2001) validated the method in vitro, with an artificial eye and in vivo with four participants with intraocular lenses. The combination of the reproducibility and systematic errors has been estimated as approximately 0.3 mm for the anterior lens and 0.25 mm for the posterior lens surface.

Participants

Experiments were performed on the right eye of 46 normal participants with ages ranging between 22 and 60 years (30 ± 9 years, mean and standard deviation). Spherical equivalent ranged from −7.25 to 4.25 D (−1.5 ± 2.5 D). The experimental protocols followed the tenets declaration of Helsinki and had been approved by institutional review boards. Participants were informed on the nature of the experiments and provided written consent.

A subsample of 11 participants (ages ranging from 22 to 36 years, mean 28.5) was also measured as a function of accommodation stimulus.

Experimental procedures

The right eye of the participants was dilated with one drop tropicamide and one drop of 5% phenylephrine HCl. For those 11 participants who were also measured as a function of accommodation stimulus, only two drops of 5% phenylephrine were used. Subsequently, refractive error and keratometry was measured with a Topcon KR-3500 auto-kerato-refractometer. Purkinje and Scheimpflug measurements were obtained in turns in the same experimental session. The participant was seated with the head in upright position, and the slit beam of the Scheimpflug was vertically oriented. The left eye was used to focus a fixation stimulus while the right eye was photographed. The fixation stimulus was an illuminated black Maltese star (diameter: 5 cm), which was located 0.5 m from the left eye. Refractive error was corrected with trial lenses in a lens holder directly in front of the left eye and a +2 D lens was added as well to obtain the unaccommodated state of the eye. Participants wearing contact lenses kept the left lens in. First of all, the participant fixated with the right eye the fixation light in the Scheimpflug camera while the slit of the camera was aligned along the optical axis of the right eye. Then, the participant fixated with the left eye the Maltese star, the position of

which can be adjusted horizontally and vertically by a remote control until the participant reports that the fixation light of the Scheimpflug camera is superimposed on the center of the Maltese star. Subsequently, the internal fixation light of the camera was turned off. At that time, the participant was asked to focus on the Maltese star and two images were obtained. For 11 participants, also Scheimpflug images of the right eye were obtained as a function of accommodation. For these images, the same procedure was followed except for the fact that to induce accommodation the power of the lens in front of the left eye was reduced in steps of 1 D. Measurements were performed until the participant indicated that it was no longer possible to focus sharply on the star.

Purkinje images were obtained with the double vertical LEDs. The right eye's pupil was aligned to the optical axis of the camera by means of an X–Y–Z stage to which a chin rest was mounted. For the left eye, the set-up (lens holder, trail lenses, Maltese cross) and protocol for the accommodation experiments were identical to that used during the Scheimpflug imaging. The pupil was continuously monitored to ensure centration and convergence was corrected by changing the lateral position of the Maltese star, until the pupil was in the center of the screen.

Statistical analysis

Statistical differences of the radii of curvature between techniques for the global sample were tested using a general linear model and analysis of variance (ANOVA) for repeated measurements. To test statistical differences between techniques for each individual eye, we performed a Test of Homogeneity of Variances (for repeated measurements with the same technique). As a result, we applied ANOVA with the Bonferroni post hoc test if the variances were equal and the Welch–ANOVA with the Tamhane post hoc test if the variances were unequal. The change of radii of curvature with accommodation and differences of those between techniques were tested using ANOVA. In all cases, a significance level (p) of .05 was considered (or a confidence interval of 95%).

Results

Figure 1 shows a typical example of a Purkinje image showing double PI, PIII, and PIV (A) and an example of a corrected Scheimpflug image (B) for the same unaccommodated eye. Movie 1 shows a sequence of images between the unaccommodated and accommodated state (6 D) using Purkinje imaging. For this example, the pupil was not dilated and the stimulus was presented in the test eye (OS). Movie 2 shows a morph between the unaccommodated and accommodated state (6 D) using uncorrected distortion Scheimpflug images. For this example, the pupil was dilated and the stimulus presented in the contralateral eye.

Lens radii of curvature of the unaccommodated eye

Table 1 shows that there is a good match between anterior lens radius from Purkinje imaging and Scheimpflug imaging.

There are no significant differences between Purkinje imaging anterior radii with data processed using individual biometric (I) or model eye data (LG) (p = .072 for EE, and p = .113 for MF). The average (±SD) difference between

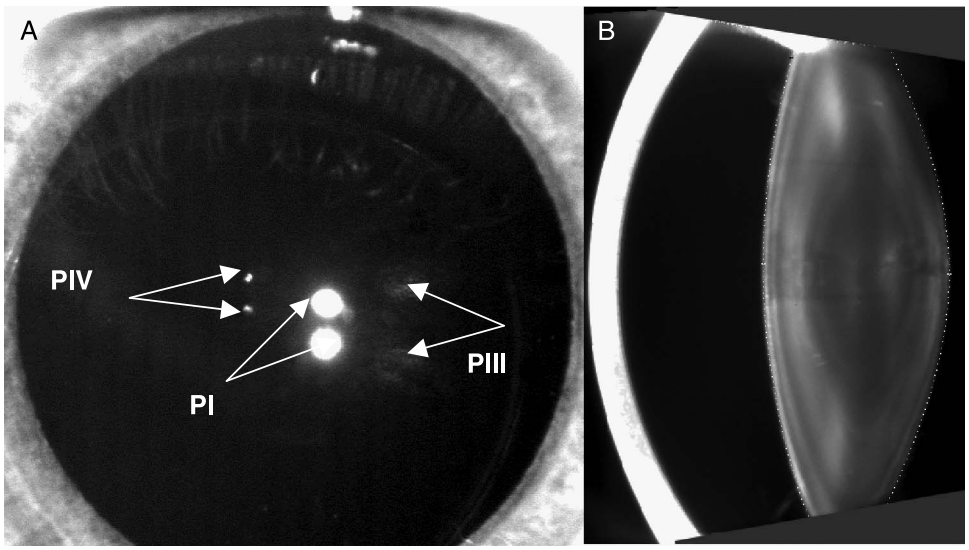

Figure 1. Examples of (A) Purkinje images (B) Scheimpflug image for the same unaccommodated eye.

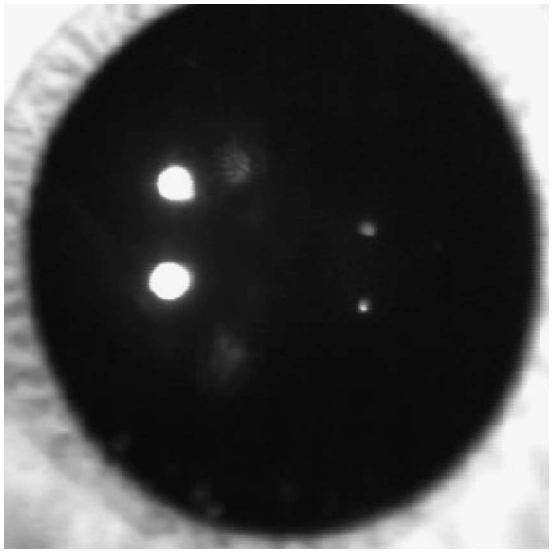

Movie 1. Examples of Purkinje images. The stimulus was presented in the test eye (OS), without dilating. Click on the image to view the movie.

the anterior lens radius obtained with Scheimpflug and Purkinje imaging MF is 0.36 ± 0.76 mm, and EE is 0.13 ± 0.77 mm.

Figure 2A shows the anterior lens radii of curvature obtained from Scheimpflug measurements versus those obtained from Purkinje imaging using the EM theorem. Solid symbols are for Purkinje imaging data using individual biometric data of anterior chamber depth and lens thickness, and open symbols are for Purkinje imaging data using fixed data from the model eye. Similarly, Figure 2B shows the same data, but with Purkinje imaging using the MF algorithm. In Figure 2, vertical error bars represent individual variability (standard deviation) for repeated Purkinje imaging anterior radii estimates. Average (across-participants) standard deviation for repeated measurements was 0.5 mm. This variability arises from an average measurement variability in h3 (separation of PIII double images) and h1 (separation of PI double images) of 0.11 mm in both cases. Horizontal error bars represent individual variability for repeated Scheimpflug imaging (and was 0.10 mm on average).

Slopes and correlation coefficients of a linear regression between anterior radii from Scheimpflug and Purkinje are very similar in all cases (slope ranging from 0.752 to 0.827, and r from .58 to .60), and the correlation is statistically significant in all cases ($p < .0001$). In an ANOVA for repeated measurements, the difference across the entire sample was not statistically significant using the EM (for both individual biometry, $p = .221$ and model eye biometry, $p = .231$). This statistical test found differences for the MF ($p = .003$ and $p = .011$ for individual and model eye biometry, respectively). On an individual basis, we found statistically significant differences in the anterior radii of curvature between techniques in 4 of the 46 eyes (using individual biometry) and 10 eyes (using model data), with the EM procedure, and 7 and 11 eyes using respectively using the MF.

Table 2 shows posterior lens radii (average ± SD and range) obtained from Scheimpflug and Purkinje imaging (with the MF and EM and individual phakometry, I, or model eye data, LG, respectively). Unlike results for the anterior lens, posterior lens radii of curvature from the MF and EM are significantly different (the EM clearly overestimating the data). The average (±SD) difference between the posterior lens radius obtained with Scheimpflug and Purkinje imaging MF is −0.57 ± 0.58 mm, and EE is −1.47 ± 0.84 mm. The difference is not increased when using nonindividual data (−0.42 mm) Table 3.

Figure 3 shows posterior radii of curvature from Scheimpflug imaging versus Purkinje imaging in a similar format to that of Figure 2. For simplicity, we show absolute values, whereas the posterior radii of curvature are always negative. Vertical error bars represent individual variability (standard deviation) for repeated Purkinje imaging posterior radii estimates. Average (across-participants) standard deviation for repeated measurements was 0.31 mm. This variability arises from an average variability in h4 (separation of PIV double images) and h1 (separation of PI double images) measurements of 0.02 mm in both cases. Horizontal error bars represent individual variability for repeated Scheimpflug imaging (and was 0.22 mm on average).

We have also estimated the differences in crystalline lens surface power resulting from the differences in anterior and posterior radii of curvature across techniques. We have used the lens maker formula, using individual data of lens thickness and equivalent refractive index obtained from Scheimpflug. For MF and LG, we estimated that Purkinje/Scheimpflug differences in anterior lens radius of 0.3 mm and posterior lens radius of −0.45 mm will result in differences in lens power of 0.61 D.

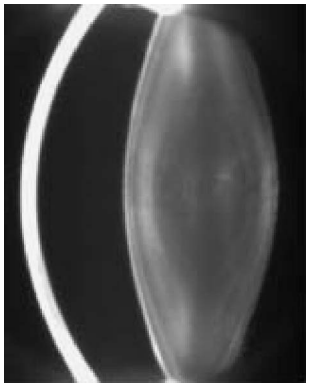

Movie 2. Examples of Scheimpflug image (accommodation range from 0 to 6 D). The pupil stimulus was presented in the contralateral eye (OS) and the pupil was dilated. Click on the image to view the movie.

Anterior lens radius	Scheimpflug camera	Purkinje imaging system			
		Individual biometric data		Model eye	
		MF	EMT	MF	EMT
Average	11.1 ± 1.1	10.8 ± 1.1	10.95 ± 1.1	10.8 ± 1.3	10.9 ± 1.25
Range	8.1, 13.8	7.9, 13.3	8.1, 13.6	7.2, 13.45	7.4, 13.5

Table 1. Comparison of the anterior lens radii of curvature in mm (mean and standard deviation) obtained with Scheimpflug and Purkinje imaging.

Slopes and correlation coefficients of a linear regression between the posterior radius obtained with Scheimpflug and Purkinje imaging are very similar in all cases (ranging from a slope of 1 to 1.09, and r from .48 to .43, $p < .0001$). In an analysis of variance, the difference across the entire samples was statistically significant for both the EM and MF ($p < .01$ in all cases). On an individual basis, we found statistically significant differences in the posterior radii of curvature between techniques in 17 and 19 of 34 using individual biometry and model data respectively, for the EM method, and in 10 and 9 participants, respectively, for the MF.

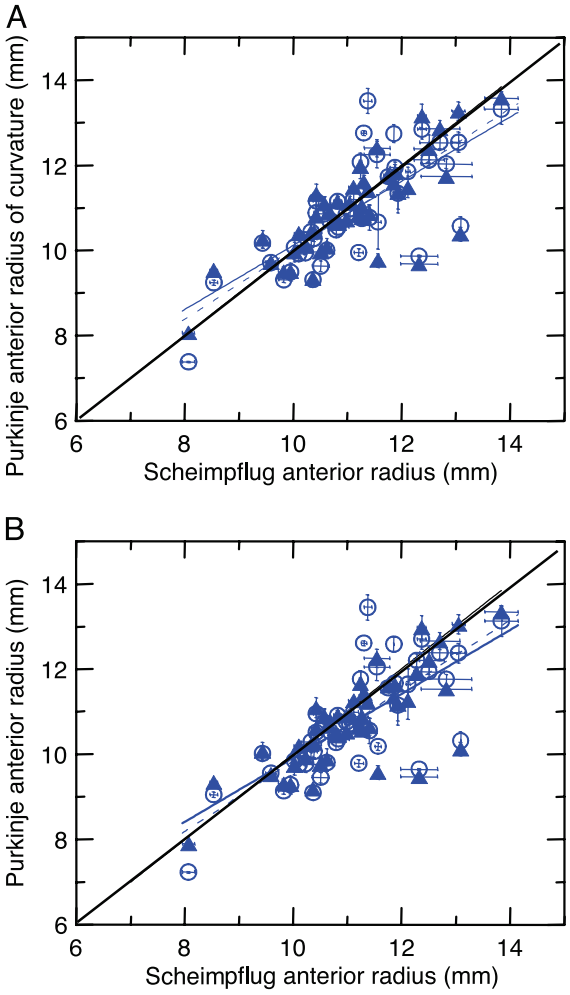

Figure 2. Anterior radii of curvature from Scheimpflug imaging versus Purkinje imaging using (A) MF and (B) EM. Solid triangles are for Purkinje imaging using individual biometry and open circles are for Purkinje imaging using biometry from a model eye.

We did not observe a consistent trend of Scheimpflug/Purkinje discrepancy as a function of accommodation (Figure 4). For the anterior lens, the Purkinje radii were slightly lower than those of the Scheimpflug in all eyes (on average across participants and accommodation by 0.39 ± 012 mm and 0.46 ± 014 mm, using individual biometry and model eye data, respectively). For the posterior lens, the Purkinje radii were slightly higher than those of the Scheimpflug in all eyes (average ± SD across participants and accommodation was 0.38 ± 0.24) (Figure 5).

In an analysis of variance (ANOVA), the difference in the anterior and posterior curvature radius obtained with the two methods was not significant ($F = 3.7$, $df = 1$, $p = .083$), whereas the difference of radii of curvature across the different accommodative states was significant ($F = 231.8$, $df = 6$, $p = .00005$).

Discussion

We found good correspondence of lens radii of curvature with our implementations of Scheimpflug and Purkinje imaging systems on the same group of eyes. The ranges of radii of curvature found with both techniques are consistent to those reported before in normal eyes for the unaccommodated eye and under different levels of accommodation stimuli. Although previous studies on different populations and different experimental protocols, and the lack of a gold standard for calibration, prevented to validate the accuracy of the different techniques used for phakometry, our comparison on an individual basis allows to identify potential systematic errors associated to a given technique and assess the potential advantages or limitations of the different techniques.

We found that Scheimpflug and Purkinje imaging (with EM) provided statistically similar results for the anterior radius of curvature. As previously suggested (Rosales &

Posterior lens radius	Scheimpflug camera	Purkinje imaging system			
		Individual biometric data		Model eye	
		MF	EMT	MF	EMT
Average	6.1 ± 0.55	6.7 ± 0.8	7.6 ± 1.0	6.5 ± 1.0	7.4 ± 1.2
Range	5.1, 7.15	5.2, 8.65	8.7, 10.2	4.8, 9.5	5.2, 11.5

Table 2. Comparison of the anterior lens radii of curvature in mm (mean and standard deviation) obtained with Scheimpflug and Purkinje imaging.

Marcos, 2006), Purkinje imaging overestimates the posterior radius of curvature. The MF provides a more accurate estimate than the EM theorem, most likely because the latter is affected by the finite distance between the light source and the eye (Hemenger et al., 1995). We have also shown that using individual biometry data increases slightly the similarity between techniques for the anterior radius, and only marginally for the posterior radius, with respect of using general data from the model eye.

We have performed computer simulations to assess whether there are systematic differences that can be attributed to the Purkinje imaging method, or that the errors do not follow any particular trend and can be attributed to both methods. The details of the ray tracing of our apparatus and computer simulations of Purkinje images were described in a previous publication (Rosales & Marcos, 2006). In brief, we simulated with Zemax the configuration of the optical system and simulated the intensity distributions of the Purkinje images for a model eye. The simulated Purkinje images were processed as the experimental images, using the MF. For the present simulations, we used as nominal values for the model eyes (biometry and radii of curvature of the cornea and anterior and posterior lens) those obtained from Scheimpflug imaging. We performed simulations for model eyes with spherical surfaces (as assumed in the processing algorithms) and also aspherical surfaces, with asphericities (Q values) obtained from Scheimpflug imaging in each individual eye (−0.26 ± 0.19 for the anterior cornea, −0.49 ± 0.19 for the posterior cornea, −2.00 ± 0.15 for the anterior lens, −2.65 ± 1.42 for the posterior lens). The simulations were performed for 31 eyes. For the anterior radii of curvature, predictions using spherical surfaces in the model eye reveal a slight underestimation of Purkinje radii compared to Scheimpflug radii of curvature (nominal values in the

	Scheimpflug	Purkinje imaging system (MF)	
		Individual biometry	Model eye
Anterior lens			
Range	(11.54, 7.26)	(11.03, 6.9)	(11.04, 6.78)
Slope	−0.64	−0.57	−0.57
Posterior lens			
Range	(6.24, 4.7)	(7.28, 5.05)	(6.81, 5.23)
Slope	−0.23	−0.29	−0.29

Table 3. Range of variation of the anterior and posterior radii of curvature between 0 and 8 D and slope of the linear regression to the data, from Scheimpflug and Purkinje imaging.

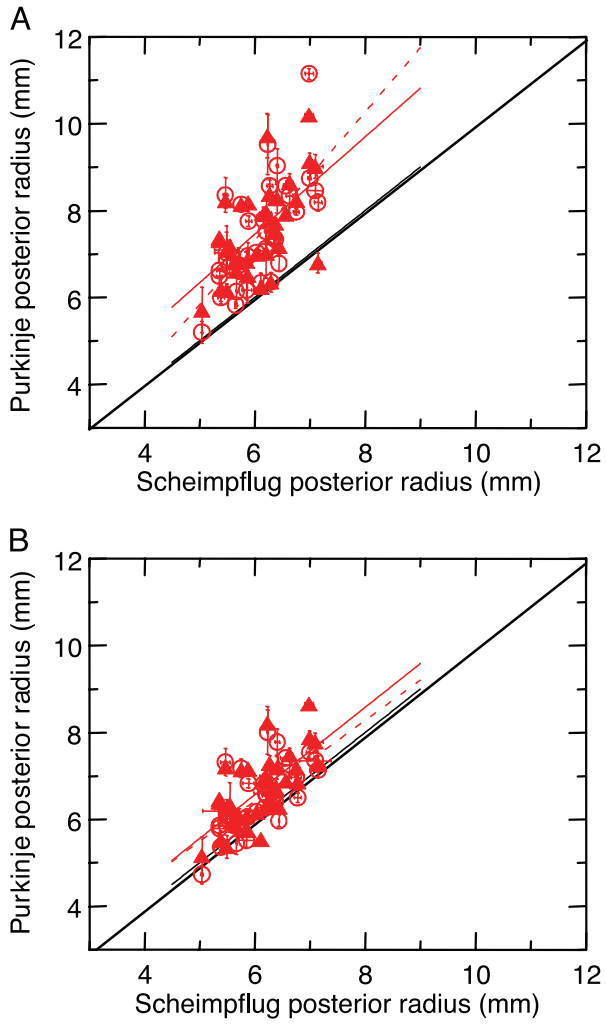

Figure 3. Posterior lens radii of curvature from Scheimpflug imaging versus Purkinje imaging using (A) MF and (B) EM. Solid triangles are for Purkinje imaging using individual biometry and open circles are for Purkinje imaging using biometry from a model eye.

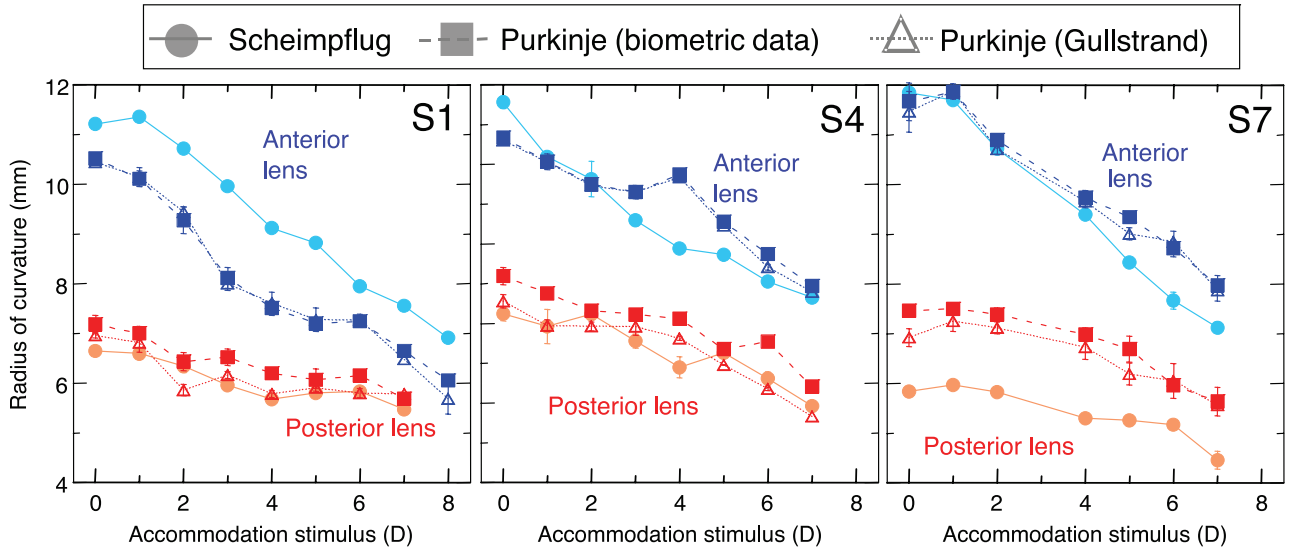

Figure 4. Change of anterior and posterior lens radii of curvature as a function of accommodation in three individual eyes.

model). However, similarly to the experimental findings, these differences are not significant. The average differences between Purkinje imaging and Scheimpflug anterior radii of curvature were 0.28 ± 0.67 mm for the experimental values in these set of eyes, −0.50 ± 0.16 for the predicted values using spherical surfaces, and −0.34 ± 0.25 for the predicted values using aspherical surfaces. There are good correlations between Scheimplug and Purkinje data. For the spherical surface model, we found a slope closer to 1 (0.93) than for the experimental (0.81) or predictions (0.87) using the aspheric model. For the posterior radius of curvature predictions with the aspheric model reproduce, a systematic overestimation of Purkinje imaging data from the nominal Scheimpflug data. A lower overestimation is found for the spherical model eye. The average differences between Purkinje imaging and Scheimpflug posterior radii

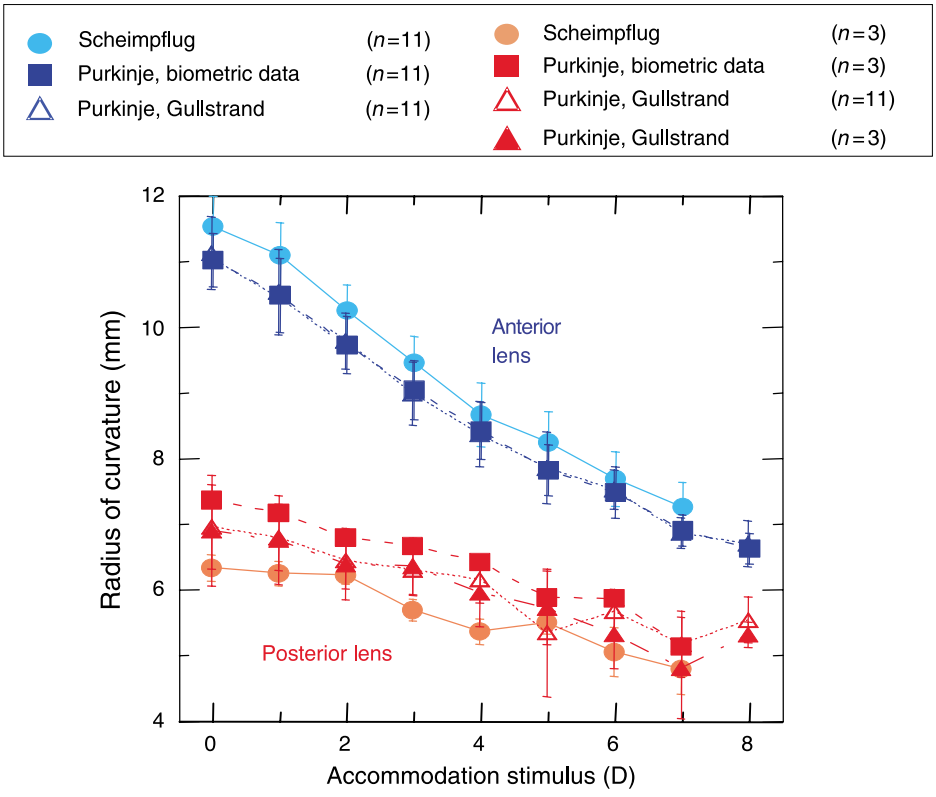

Figure 5. Change of anterior and posterior lens radii of curvature as a function of accommodation, averaged across eyes.

of curvature were 0.60 ± 0.57 for the experimental values, 0.48 ± 0.43 for the predicted values using spherical surfaces, and 1.04 ± 0.69 for the predicted values using aspherical surfaces. These simulations indicate that the discrepancies found between the Purkinje and Scheimpflug posterior radii are partly inherent to the method, and also to the fact that the surface of the crystalline lens is not spherical, but exhibits a negative asphericity (with nominal values obtained from Scheimpflug). The larger the asphericity, the larger the discrepancy. Thus, the simulations predict a higher overestimation of the lens radii, whereas the experimental values lie in between predictions from spherical and aspheric surfaces. This could indicate that the asphericity of the lens is actually lower (more spherical) or that the gradient index of the lens could play a counteractive role. The asphericity of the anterior surface does not seem to affect the estimation of the anterior lens radius using Purkinje imaging, but the asphericity of the anterior lens surface, posterior lens surface, or both do play a substantial large role in the slight overestimation of the Purkinje radii of curvature. The asphericity of the crystalline lens surfaces in young eyes is usually negative (Dubbelman et al., 2005) but varies significantly across participants and as a function of accommodation. The MF could incorporate an aspheric eye model to account for some of this effect, although a fixed asphericity will probably not account for all the individual effects.

Both techniques provided rapid and reliable data in a clinical/laboratory setting. Scheimpflug imaging turned out to be slightly less variable than Purkinje imaging across repeated measurements. Both techniques require some degree of pupil dilation. Using Purkinje imaging, it was possible to measure the radius of the anterior and posterior lens surface for all eyes, whereas in 14 eyes the pupil was not wide enough to obtain the posterior radius using Scheimpflug imaging. With accommodation, the pupil constricts and the lens becomes thicker, which makes the measurement of the posterior lens surface even more difficult for the Scheimpflug imaging. Other advantages of the Purkinje imaging are the simplicity of the optical set-up, which can be incorporated to other optical systems and its affordability. On the other hand, Scheimpflug imaging provides much more complete information on anterior chamber biometry and the crystalline lens geometry, beyond radii of curvature which makes it attractive to investigate the sources of variability in the optical properties of individual eyes, and their changes with accommodation or aging.

Acknowledgments

This study was supported by European Young Investigator Award (EURYI) 2005 Award to Susana Marcos and by grant # FIS2005-04382 (Ministerio de Educación y Ciencia, España) and by a grant of the Ministry of Economic Affairs, The Hague (Senter grant ISO 43081, Advanced Medical Optics, Groningen, The Netherlands) to Rob van der Heijde and Michiel Dubbelman. Patricia Rosales was supported by an FPI predoctoral fellowship BFM-2002-02638 and a visiting fellowship from Ministerio de Educación y Ciencia, España).

Commercial relationships: none.
Corresponding author: Patricia Rosales.
Email: Patricia@io.cfmac.csic.es.
Address: Instituto de Optica, "Daza de Valdés," Consejo Superior de Investigaciones Científicas, Madrid, Spain.

References

Barry, J. C., Dunne, M., & Kirschkamp, T. (2001). Phakometric measurement of ocular surface radius of curvature and alignment: Evaluation of method with physical model eyes. *Ophthalmic & Physiological Optics, 21,* 450–460. [PubMed]

Brown, N. (1974). The change in lens curvature with age. *Experimental Eye Research, 19,* 175–183. [PubMed]

Dubbelman, M., Sicam, V. A., & Van der Heijde, G. L. (2006). The shape of the anterior and posterior surface of the aging human cornea. *Vision Research, 46,* 993–1001. [PubMed]

Dubbelman, M., van der Heijde, G. A., & Weeber, H. A. (2001). The thickness of the aging human lens obtained from corrected Scheimpflug images. *Optometry and Vision Science, 78,* 411–416. [PubMed] [Article]

Dubbelman, M., & Van der Heijde, G. L. (2001). The shape of the aging human lens: Curvature, equivalent refractive index and the lens paradox. *Vision Research, 41,* 1867–1877. [PubMed]

Dubbelman, M., Van der Heijde, G. L., & Weeber, H. A. (2005). Change in shape of the aging human crystalline lens with accommodation. *Vision Research, 45,* 117–132. [PubMed]

Fink, W. (2005). Refractive correction method for digital charge-coupled device-recorded Scheimpflug photographs by means of ray tracing. *Journal of Biomedical Optics, 10,* 024003. [PubMed]

Garner, L. F., Ooi, C. S., & Smith, G. (1998). Refractive index of the crystalline lens in young and aged eyes. *Clinical & Experimental Optometry, 81,* 145–150. [PubMed]

Garner, L. F. (1997). Calculation of the radii of curvature of the crystalline lens surfaces. *Ophthalmic & Physiological Optics, 17,* 75–80. [PubMed]

Garner, L. F., & Smith, G. (1997). Changes in equivalent and gradient refractive index of the crystalline lens with accommodation. *Optometry and Vision Science, 74,* 114–119. [PubMed]

Garner, L. F., & Yap, M. K. (1997). Changes in ocular dimensions and refraction with accommodation. *Ophthalmic & Physiological Optics, 17,* 12–17. [PubMed]

Glasser, A., Wendt, M., & Ostrin, L. (2006). Accommodative changes in lens diameter in rhesus monkeys. *Investigative Ophthalmology & Visual Science, 47,* 278–286. [PubMed]

Guirao, A., & Artal, P. (2000). Corneal wave aberration from videokeratography: Accuracy and limitations of the procedure. *Journal of the Optical Society of America A, Optics, Image Science, and Vision, 17,* 955–965. [PubMed]

Guirao, A., Redondo, M., & Artal, P. (2000). Optical aberrations of the human cornea as a function of age. *Journal of the Optical Society of America A, Optics, Image Science, and Vision, 17,* 1697–1702. [PubMed]

He, J. C., Gwiazda, J., Thorn, F., Held, R., & Vera-Diaz, F. A. (2005). The association of wavefront aberration and accommodative lag in myopes. *Vision Research, 45,* 285–290. [PubMed]

Hemenger, R. P., Garner, L. F., & Ooi, C. S. (1995). Change with age of the refractive index gradient of the human ocular lens. *Investigative Ophthalmology & Visual Science, 36,* 703–707. [PubMed]

Holladay, J. T., Piers, P. A., Koranyi, G., van der Mooren, M., & Norrby, N. E. (2002). A new intraocular lens design to reduce spherical aberration of pseudophakic eyes. *Journal Refractive Surgery, 18,* 683–691. [PubMed]

Huebscher, H., Fink, W., Steinbruck, D., & Seiler, T. (1999). Scheimpflug records without distortion—A mythos? *Ophthalmic Research, 31,* 134–139. [PubMed]

Kampfer, T., Wegener, A., Dragomirescu, V., & Hockwin, O. (1989). Improved biometry of the anterior eye segment. *Ophthalmic Research, 21,* 239–248. [PubMed]

Koretz, J. E., Strenk, S. A., Strenk, L. M., Semmlow, J. L. (2005). Comment in Scheimpflug and high-resolution magnetic resonance imaging of the anterior segment: A comparative study. *Journal of the Optical Society of America A, Optics, Image Science, and Vision, 22,* 1216–1218. [PubMed]

Koretz, J. E., Cook, C. A., & Kaufman, P. L. (2002). Aging of the human lens: Changes in lens shape upon accommodation and with accommodative loss. *Journal of the Optical Society of America A, Optics, Image Science, and Vision, 19,* 144–151. [PubMed]

Koretz, J., & Handelman, G. (1986). The lens paradox and image formation in accommodating human lenses. *Topics in Aging Research in Europe, 6,* 57–64.

Koretz, J. F., Cook, C. A., & Kaufman, P. L. (1997). Accommodation and presbyopia in the human eye. Changes in the anterior segment and crystalline lens with focus. *Investigative Ophthalmology & Visual Science, 38,* 569–578. [PubMed]

Koretz, J. F., Cook, C. A., & Kaufman, P. L. (2001). Aging of the human lens: Changes in lens shape at zero-diopter accommodation. *Journal of the Optical Society of America A, Optics, Image Science, and Vision, 18,* 265–272. [PubMed]

Le Grand, Y., & El Hage, S. G. (1980). Translation and update of Le Grand Y. (1968) "La dioptrique de l'oelil et sa correction, vol. I of Optique physiologique." *Physiological Optics, I,* 65–67.

Marcos, S., Barbero, S., McLellan, J. S., & Burns, S. A. (2003). Optical Quality of the Eye and Aging. In S. MacRae, R. Krueger, & R. Applegate (Eds.), *Custom corneal ablation: The quest for supervision*. Thornfare, NJ: Slack Publishing.

Marcos, S., Barbero, S., & Jiménez-Alfaro, I. (2005). Optical quality and depth-of-field of eyes implanted with spherical and aspheric intraocular lenses. *Journal of Refractive Surgery, 21,* 223–235. [PubMed]

Marcos, S., Burns, S. A., Moreno-Barriusso, E., & Navarro, R. (1999). A new approach to the study of ocular chromatic aberrations. *Vision Research, 39,* 4309–4323. [PubMed]

Mutti, D. O., Zadnik, K., & Adams, A. J. (1992). A video technique for phakometry of the human crystalline lens. *Investigative Ophthalmology & Visual Science, 33,* 1771–1782. [PubMed]

Phillips, P., Perez-Emmanuelli, J., Rosskothen, H. D., & Koester, C. J. (1988). Measurement of intraocular lens decentration and tilt *in vivo*. *Journal of Cataract and Refractive Surgery, 14,* 129–135. [PubMed]

Ray, S. (1995). *Applied photographic optics*. Oxford: Focal Press, 452.

Roorda, A., & Glasser, A. (2004). Wave aberrations of the isolated crystalline lens. *Journal of Vision, 4*(4), 250–261, http://journalofvision.org/4/4/1/, doi:10.1167/4.4.1. [PubMed] [Article]

Rosales, P., & Marcos, S. (2006). Phakometry and lens tilt and decentration using a custom-developed Purkinje imaging apparatus: Validation and measurements. *Journal of the Optical Society of America A, Optics, Image Science, and Vision, 23,* 509–520. [PubMed]

Scheimpflug, T. (1906). Der Photospektograph und seine Anwendung. *Photographische Korrespondenz,* 43.

Smith, G., & Garner, L. F. (1996). Determination of the radius of curvature of the anterior lens surface from the Purkinje images. *Ophthalmic and Physiological Optics, 16,* 135–143. [PubMed]

Sorsby, A., Benjamin, B., & Sheridan, M. (1961). *Refraction and its components during the growth of the eye from the age of three (No. 301)*. London: Medical Research Council Special Report Series.

Van Veen, H. G., & Goss, D. A. (1988). Simplified system of Purkinje image photography for phakometry. *American Journal of Optometry and Physiological Optics, 65,* 905–908. [PubMed]

Wulfeck, J. W. (1955). Infrared Photography of the so-called third Purkinje image. *Journal of the Optical Society of America, 45,* 928–930. [PubMed]

Zadnik, K., Mutti, D. O., Mitchell, G. L., Jones, L. A., Burr, D., & Moeschberger, M. L. (2004). Normal eye growth in emmetropic schoolchildren. *Optometry and Vision Science, 81,* 819–828. [PubMed] [Article]